A Fast Algorithm and its Application to Computing Pulsatile Flow in an Eccentric Catheterized Artery

Prabir Daripa* and Ranjan K. Dash
Department of Mathematics, Texas A&M University, College Station, TX–77843

Abstract

The pulsatile flow in an eccentric catheterized artery is studied numerically by making use of an extended version of the fast algorithm recently developed by Borges and Daripa [3]. The flow rate is prescribed as a periodic function of time. The axial pressure gradient and axial velocity distribution in the catheterized artery are obtained as solutions of the problem. Through the computed results, the increases in mean pressure gradient and mean frictional resistance in the artery due to catheterization are estimated.

1 Introduction

Catheters attached with various functional tools have extensive use in contemporary medical sciences. The measurement of various physiological flow characteristics (e.g., arterial blood pressure or pressure gradient and flow velocity or flow rate) as well as the diagnosis (e.g., X-ray angiography and intravascualar ultrasound) and treatment (e.g., coronary balloon angioplasty) of various arterial diseases are done through an appropriate catheter-tool device by inserting the device into a peripheral artery and positioning it in the desired part of the arterial network (see Back [1], Back et al. [2], and Dash et al. [7, 8] for details).

The insertion of a catheter into an artery leads to the formation of an annular region between the catheter wall and the arterial wall. This will increase the flow resistance in the artery and modify the pressure distribution. Therefore, the pressure/pressure gradient recorded by a transducer attached to the catheter will differ from that of an uncatheterized artery. In order to obtain an accurate pressure reading, it is essential to know the catheter-induced errors. This necessitates a study of blood flow in a catheterized artery.

Through a detailed mathematical model, MacDonald [11] studied the pulsatile flow in an eccentric catheterized artery and obtained the estimates for pressure gradient corrections. Back [1] and Back et al. [2] studied the important hemodynamical characteristics like the wall shear stress, pressure drop, and frictional resistance in a catheterized coronary artery under normal as well as stenosed conditions and estimated the mean flow resistance increase due to catheterization. Taking into account the non-Newtonian nature of blood, Dash et al. [7] studied the flow pattern in a narrow catheterized artery and estimated the increased frictional resistance in the artery due to catheterization. The effect of catheterization on various flow characteristics in a curved artery with or without stenosis was studied by Karahalios [10], Jayaraman and Tiwari [9], and Dash et al. [8].

In this paper, we revisit the problem of pulsatile blood flow in a straight eccentric catheterized artery which was originally studied by MacDonald [11]. However, here we compute the flow characteristics (i.e., the axial pressure gradient and axial velocity distribution) *accurately* and *rapidly* by using an extended version of the fast algorithm developed recently by Borges and Daripa [3] (see also Daripa and collaborators [4, 5]). Through the computed results, we estimate the increases in mean pressure gradient and frictional resistance in the artery due to catheterization. A more detailed exposition of the material presented here can be found in Daripa and Dash [6].

2 Mathematical formulation

Figure 1 shows a typical cross-section of the catheterized artery. It is an eccentric annular region Ω bounded by $\partial\Omega = \Gamma_1 \cup \Gamma_2$ where

$$\Gamma_1 : \; x^2 + y^2 = r_0^2 \quad \text{and} \quad \Gamma_2 : \; (x-b)^2 + y^2 = r_i^2. \tag{2.1}$$

*Author for correspondence (E-mail: Prabir.Daripa@math.tamu.edu)

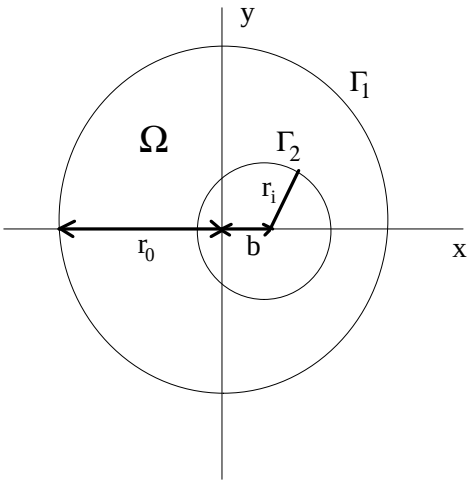

Figure 1: Schematic diagram of a cross-sectional plane of the eccentric catheterized artery.

Here r_0 and r_i are the radii of the outer (artery) and inner (catheter) tubes respectively. The origin $(0,0)$ of the coordinate system is chosen as the center of the outer tube and the x-axis is chosen to pass through the center of the inner tube in the cross-sectional plane. We denote the center of the inner tube as $(b,0)$. The axial flow in the eccentric annulus is considered to be due to an uniform pulsatile (oscillatory) axial pressure gradient $\frac{\partial p}{\partial z}(t)$ with period $\frac{2\pi}{\omega}$. The velocity field is given by $(0,0,w)$. The fluid (blood) is considered to be incompressible and Newtonian, and the flow is assumed to be laminar and fully developed. Then the simplified Navier-Stokes equation and the no-slip boundary conditions for the flow (see MacDonald [11]) are given by

$$\rho\frac{\partial w}{\partial t} = -\frac{\partial p}{\partial z} + \mu\left[\frac{\partial^2 w}{\partial x^2} + \frac{\partial^2 w}{\partial y^2}\right] \quad \text{in} \quad \Omega, \tag{2.2}$$

and

$$w = 0 \quad \text{on} \quad \partial\Omega, \tag{2.3}$$

where ρ and μ are density and viscosity of the fluid respectively. It is convenient to work with non-dimensional variables. Therefore, we introduce the characteristics length as r_0, characteristics pressure gradient as $-P_g$ (mean pressure gradient), characteristic velocity as $P_g r_0^2/\mu$, and the characteristics time as ω^{-1}. In non-dimensional form (retaining the same notations), equations (2.1) and (2.2) are reduced to

$$\alpha^2\frac{\partial w}{\partial t} = \frac{\partial p}{\partial z} + \frac{\partial^2 w}{\partial x^2} + \frac{\partial^2 w}{\partial y^2} \quad \text{in} \quad \Omega, \tag{2.4}$$

and

$$w = 0 \quad \text{on} \quad \partial\Omega, \tag{2.5}$$

where $\alpha = \sqrt{r_0^2\omega/(\frac{\mu}{\rho})}$ is the Womersley frequency parameter. The boundary curves Γ_1 and Γ_2, in non-dimensional form, are now given by

$$\Gamma_1 \colon\ x^2 + y^2 = 1 \quad \text{and} \quad \Gamma_2 \colon (x-c)^2 + y^2 = a^2, \tag{2.6}$$

where $a = r_i/r_0$ and $c = b/r_0$. During flow simulation in a catheterized artery, it is often desirable to estimate the increase in axial pressure gradient due to the insertion of a catheter into an artery. In this case, the flux (flow rate) is assumed to be known (constant) which can be expressed in the form of Fourier series

$$Q(t) \ = \ \iint\limits_{\Omega} w(x,y,t)dxdy \ = \ \sum_{j=-\infty}^{\infty} Q_j e^{ijt}, \tag{2.7}$$

where $i = \sqrt{-1}$. The flow-rate is non-dimensionalized with respect to the characteristics flow rate $P_g r_0^4/\mu$.

3 Method of solution

Since the flow rate $Q(t)$ is a periodic function of time t (prescribed), we seek the solutions for $\frac{\partial p}{\partial z}(t)$ and $w(x, y, t)$ in the form of Fourier series

$$\frac{\partial p}{\partial z}(t) = \sum_{j=-\infty}^{\infty} P_j e^{ijt}, \quad \text{and} \quad w(x, y, t) = \sum_{j=-\infty}^{\infty} w_j(x, y) e^{ijt}. \tag{3.1}$$

Substituting the series (3.1) in the Dirichlet problem comprising of equations (2.4) and (2.5) and equating the coefficients of e^{ijt} on both the sides, we get the Dirichlet problem

$$\frac{\partial^2 E_j}{\partial x^2} + \frac{\partial^2 E_j}{\partial y^2} = i\gamma_j E_j - 1 \quad \text{in} \quad \Omega, \tag{3.2}$$

and

$$E_j = 0 \quad \text{on} \quad \partial\Omega, \tag{3.3}$$

for $j = 0, \pm 1, \pm 2, \cdots, \pm\infty$. Here $E_j(x, y) = w_j(x, y)/P_j$ and $\gamma_j = j\alpha^2$. It can be easily shown that the coefficients E_j's satisfy $E_j = \overline{E_{-j}}$ for $j = \pm 1, \pm 2, \cdots, \pm\infty$. It is worth noting here that the equation (3.2) is a complex Helmholtz equation for the complex coefficient E_j. Solving the Dirichlet problem (3.2) and (3.3) provides E_j which can be used, as described below, to obtain the axial pressure gradient in the eccentric annulus.

3.1 Evaluation of Pressure Gradient

Substituting the expression (3.1) for $w(x, y, t)$ in equation (2.7) and equating the coefficient of e^{ijt} on both the sides, we get

$$\iint_{\Omega} w_j(x, y) dx dy = Q_j, \tag{3.4}$$

which gives

$$P_j = Q_j \Big/ \iint_{\Omega} E_j(x, y) dx dy, \tag{3.5}$$

for $j = 0, \pm 1, \pm 2, \pm\infty$. The axial pressure gradient in the eccentric annulus can be obtained through equations (3.1) and (3.5).

In the following subsection, we describe our approach for solving the Dirichlet problem comprising of the complex Helmholtz equation (3.2) and the boundary condition (3.3) in the eccentric annular domain Ω. In order to take advantage of recently developed fast solvers (described in section 4) for real elliptic problems which are well suited for concentric circles, we first conformally transform the eccentric annular domain Ω into a concentric annular domain D and then transform the complex Helmholtz equation into a two coupled Poisson equations. We discuss this procedure next.

3.2 Conformal Mapping

It is easy to see that the conformal mapping (see MacDonald [11])

$$\xi = f(z) = \frac{z - \beta_1}{z - 1/\beta_1}, \tag{3.6}$$

maps the circles $\Gamma_1 \colon\ |z| = 1$ and $\Gamma_2 \colon\ |z - c| = a$ into the circles $\partial D_1 \colon\ |\xi| = \beta_1$ and $\partial D_2 \colon\ |\xi| = \beta_2$, respectively, where β_1 is the smallest real root of the quadratic algebraic equation

$$cs^2 + (a^2 - c^2 - 1)s + c = 0, \tag{3.7}$$

and

$$\beta_2 = \sqrt{\frac{\beta_1(\beta_1 - c)}{1 - \beta_1 c}}. \tag{3.8}$$

It is easy to check that if $c > 0$ and $a + c < 1$, then

$$0 < c < \beta_1 < a + c < 1 \quad \text{and} \quad 0 < \beta_2 < \beta_1. \tag{3.9}$$

Therefore, the eccentric annular region Ω bounded by the circles Γ_1 and Γ_2 in z-plane is mapped onto the concentric annular region D bounded by $\partial D = \partial D_1 \cup \partial D_2$ in the ξ-plane. If we denote $\xi = re^{i\theta}$, then the conformal mapping (3.6) transforms the Dirichlet problem (3.2) and (3.3) into

$$\Delta E_j = F(r,\theta)(i\gamma_j E_j - 1) \quad \text{in} \quad D, \tag{3.10}$$

and

$$E_j = 0 \quad \text{on} \quad \partial D, \tag{3.11}$$

where the Laplacian Δ and the function $F(r,\theta)$ are defined, respectively, by

$$\Delta = \frac{\partial^2}{\partial r^2} + \frac{1}{r}\frac{\partial}{\partial r} + \frac{1}{r^2}\frac{\partial^2}{\partial \theta^2}, \tag{3.12}$$

and

$$F(r,\theta) = \left|\frac{\beta_1^2 - 1}{\beta_1(\xi - 1)^2}\right|^2 = \frac{(\beta_1^2 - 1)^2}{\beta_1^2(1 - 2r\cos\theta + r^2)^2}. \tag{3.13}$$

The expression (3.5) for the Fourier coefficient P_j is transformed into

$$P_j = Qj \Big/ \int_0^{2\pi}\int_{\beta_2}^{\beta_1} F(r,\theta)E_j(r,\theta)r\,dr\,d\theta. \tag{3.14}$$

3.3 Precise Mathematical Problem and Numerical Scheme

For convenience, we write the function $E_j(r,\theta)$ in the form

$$E_j(r,\theta) = G_j(r,\theta) + iH_j(r,\theta). \tag{3.15}$$

Then the Dirichlet problem (3.10) and (3.11) is reduced to

$$\left.\begin{aligned} \Delta G_j &= -F(r,\theta)(\gamma_j H_j + 1) \\ \Delta H_j &= F(r,\theta)\gamma_j G_j \end{aligned}\right\} \quad \text{in} \quad D, \tag{3.16}$$

and

$$G_j = H_j = 0 \quad \text{on} \quad \partial D. \tag{3.17}$$

The above Dirichlet problem comprising of the two coupled Poisson equations (3.16) and boundary conditions (3.17) is numerically solved through the following iterative scheme

$$\left.\begin{aligned} \Delta G_j^{(k+1)} &= -F(r,\theta)(\gamma_j H_j^{(k)} + 1) \\ \Delta H_j^{(k+1)} &= F(r,\theta)\gamma_j G_j^{(k+1)} \end{aligned}\right\} \quad \text{in} \quad D, \tag{3.18}$$

subject to conditions

$$G_j^{(k+1)} = 0 = H_j^{(k+1)} \quad \text{on} \quad \partial D. \tag{3.19}$$

The initial guess $G_j^{(1)}(r,\theta) = H_j^{(1)}(r,\theta) = 0,\ \forall\ (r,\theta) \in D$ is chosen to start the iteration procedure. The iteration is continued until following convergence criterion is met.

$$\left.\begin{aligned} \|G_j^{(k+1)}(r,\theta) - G_j^{(k)}(r,\theta)\|_\infty &\le \epsilon \\ \|H_j^{(k+1)}(r,\theta) - H_j^{(k)}(r,\theta)\|_\infty &\le \epsilon \end{aligned}\right\}. \tag{3.20}$$

The above numerical scheme requires solving two Poisson equations in each iteration for each j. Therefore we need to solve approximately $2KL$ number of Poisson equations where K is the number of Fourier coefficients used for numerical purposes and L is the average number of iterations required for each j in the above iteration. Since this could be expensive numerically, in particular if K and/or L are large, we adapt a recently developed fast algorithm for the Poisson equation in a circular disk by Borges and Daripa [3] to our annular region with appropriate modification. We discuss this algorithm next.

4 A Fast Algorithm for the Poisson Equation in an Annular Disk

In this section, we present a fast algorithm for the Poisson equation in an annular disk with Dirichlet boundary condition which is used in the iteration scheme (3.18) and (3.19). Various fast algorithms to solve elliptic equations exist, but here we use the one originally developed by Daripa and co-workers [3, 4, 5] for this kind of problems. In Borges and Daripa [3], a fast algorithm is presented to solve the Poisson equation in a circular disk with Dirichlet and Neumann boundary condition. Here that algorithm is modified suitably to extend it to an annular disk. We consider the problem

$$\left.\begin{array}{ll} \Delta w = f(r,\theta) & \text{in } D \\ w = g(\theta) & \text{on } \partial D \end{array}\right\}, \tag{4.1}$$

where $D = \{\xi \in \mathbb{R}^2 : \ \beta_1 < |\xi| < \beta_2\}$ and $\partial D = \{\xi \in \mathbb{R}^2 : \ |\xi| = \beta_1 \text{ or } |\xi| = \beta_2\}$. Let

$$g(\theta) = \begin{cases} g_1(\theta), & \text{if } \xi = \beta_1 e^{i\theta}, \\ g_2(\theta), & \text{if } \xi = \beta_2 e^{i\theta}, \end{cases} \quad \theta \in [0, 2\pi]. \tag{4.2}$$

We can express the solution of the problem (4.1) in the form

$$w(r,\theta) = u(r,\theta) + v(r,\theta), \tag{4.3}$$

where $u(r,\theta)$ and $v(r,\theta)$ satisfy, respectively,

$$\Delta u = f(r,\theta) \quad \text{in} \quad D, \tag{4.4}$$

and

$$\left.\begin{array}{ll} \Delta v = 0 & \text{in } D \\ v = g - u & \text{on } \partial D \end{array}\right\}. \tag{4.5}$$

In sections 4.1 and 4.2, we present the fast algorithms to find a solution of (4.4) and to solve the problem (4.5).

4.1 A Solution of Equation (4.4)

A particular solution of equation (4.4) can be written as

$$u(\xi) = \iint_D f(\eta) G(\xi,\eta) d\eta_1 d\eta_2, \quad \xi \in D, \tag{4.6}$$

where

$$G(\xi,\eta) = \frac{1}{2\pi} \log|\xi - \eta|, \tag{4.7}$$

is the free-space Green's function for the Laplacian in the domain D; $\xi = \xi_1 + i\xi_2$ and $\eta = \eta_1 + i\eta_2$. For numerical evaluation of the singular integral in equation (4.6), the annular domain D is divided into a grid formed by a set of radial lines and concentric circular lines. The use of standard quadrature rules to evaluate the integral leads to poor accuracy. Moreover, complexity of the quadrature method is $O(N^4)$ for a N^2 grid points in the annular domain D. For large N, the method becomes expensive in terms of computational time. However, the integrals in equation (4.6) can be computed accurately and rapidly by extending the fast algorithm originally developed by Daripa and co-workers [3, 4, 5] to the annular domain.

The mathematical foundation of the fast algorithm to evaluate (4.6) is embedded in the following theorem. Here, we represent the solution $u(r,\theta)$ as a Fourier series with radius dependent Fourier coefficients $u_n(r)$. These Fourier coefficients $u_n(r)$ are obtained in terms of one-dimensional integrals in radial direction. The proof of the theorem is given in Daripa and Dash [6]. This theorem is based on a minor modification of the proof given in Borges and Daripa [3] for a circular disk.

Theorem 1. *If $f_n(r)$ is the nth Fourier coefficient of the function $f(r,\theta)$, then the nth Fourier coefficient $u_n(r)$ of the solution $u(r,\theta)$ can be written as*

$$u_n(r) = \int_{\beta_2}^{r} p_n(r,\rho) d\rho + \int_{r}^{\beta_1} q_n(r,\rho) d\rho, \tag{4.8}$$

where

$$p_n(r,\rho) = \begin{cases} \rho \log r f_0(\rho), & n = 0, \\ -\dfrac{\rho}{2|n|}\left(\dfrac{\rho}{r}\right)^{|n|} f_n(\rho), & n \neq 0, \end{cases} \tag{4.9}$$

and

$$q_n(r,\rho) = \begin{cases} \rho \log \rho f_0(\rho), & n = 0, \\ -\dfrac{\rho}{2|n|}\left(\dfrac{r}{\rho}\right)^{|n|} f_n(\rho), & n \neq 0. \end{cases} \tag{4.10}$$

Despite the fact that the above theorem presents the mathematical foundation of the algorithm, an efficient implementation can be made by devising suitable recursive relations to carry out the one-dimensional integration in equation (4.8) and to evaluate the Fourier coefficients $u_n(r)$ of the solution $u(r,\theta)$. Let the annular domain $D = \{\xi \in \mathbb{R}^2 : \beta_2 \leq |\xi| \leq \beta_1\}$ be discretized into NxM grid points with N equidistant points in the angular direction and M equidistant points in radial direction. Theorem 1 leads to the following corollary.

Corollary 1. *Let $\beta_2 = r_1 < r_2 < \cdots < r_M = \beta_1$. Define*

$$C_n^{i,j} = \begin{cases} \displaystyle\int_{r_i}^{r_j} \frac{\rho}{2n}\left(\frac{r_j}{\rho}\right)^n f_n(\rho)d\rho, & n < 0, \\ \displaystyle\int_{r_i}^{r_j} \rho f_n(\rho)d\rho, & n = 0, \end{cases} \tag{4.11}$$

and

$$D_n^{i,j} = \begin{cases} \displaystyle -\int_{r_i}^{r_j} \frac{\rho}{2n}\left(\frac{r_i}{\rho}\right)^n f_n(\rho)d\rho, & n > 0, \\ \displaystyle\int_{r_i}^{r_j} \rho \log \rho f_n(\rho)d\rho, & n = 0. \end{cases} \tag{4.12}$$

Let $r_j > r_i$ and define

$$\begin{cases} u_n^-(r_1) = 0, & n \leq 0, \\ u_n^-(r_j) = \left(\dfrac{r_j}{r_i}\right)^n u_n^-(r_i) + C_n^{i,j}, & n \leq 0, \end{cases} \tag{4.13}$$

and

$$\begin{cases} u_n^+(r_M) = 0, & n \geq 0, \\ u_n^+(r_i) = \left(\dfrac{r_i}{r_j}\right)^n u_n^+(r_j) + D_n^{i,j}, & n \geq 0. \end{cases} \tag{4.14}$$

Then, for $i = 1, 2, \ldots, n$, we have

$$u_n(r_i) = \begin{cases} u_n^-(r_i) + \overline{u_{-n}^+(r_i)}, & n < 0, \\ \log(r_i) u_n^-(r_i) + u_n^+(r_i), & n = 0, \\ u_n^+(r_i) + \overline{u_{-n}^-(r_i)}, & n > 0. \end{cases} \tag{4.15}$$

The above Corollary defines the recursive relations to obtain the Fourier coefficients $u_n(r)$ of the solution $u(r,\theta)$ based on the sign of the index n of u_n. Equation (4.13) constructs $n \leq 0$ modes from the smallest radius r_1 towards the largest radius r_M. Conversely, equation (4.14) constructs $n \geq 0$ modes from r_M to r_1. The steps involved in computing a particular solution $u(r,\theta)$ of equation (4.4) in an annular region D are presented in Algorithm 1 below.

Algorithm 1: Computation of Solutions of Equation (4.4) in the Annular Domain *D*.

For a given grid size $M \times N$, equidistant grid points ($r_l = \beta_2 + (l-1)(\beta_1 - \beta_2)/(M-1), \theta_k = 2\pi k/N$), and specified grid values $f(r_l e^{i\theta_k})$, the algorithm returns the solution values $u(r_l e^{i\theta_k})$ for $l \in [1, M]$ and $k \in [1, N]$.

1. Compute the Fourier coefficients $f_n(r_l),\ n \in [-N/2, N/2]$, for each $l \in [1, M]$ of the grid data $f(r_l e^{i\theta_k}),\ l \in [1, M],\ k \in [1, N]$. FFT is used for such purposes as discussed in the note at the end of next subsection.

2. For $i \in [1, M-1]$, compute the one-dimensional radial integrals $C_n^{i,i+1},\ n \in [-N/2, 0]$, and $D_n^{i,i+1},\ n \in [0, N/2]$ as defined in equations (4.11) and (4.12) using trapezoidal rule.

3. Compute the coefficients $u_n^-(r_l),\ n \in [-N/2, 0],\ l \in [1, M]$ as defined by equation (4.13):
   (a) Set $u_n^-(r_1) = 0,\ n \in [-N/2, 0]$,
   (b) For $l = 2, \cdots, M$, compute
   $$u_n^-(r_l) = \left(\frac{r_l}{r_{l-1}}\right)^n u_n^-(r_{l-1}) + C_n^{l-1,l}, \quad n \in [-N/2, 0].$$

4. Compute the coefficients $u_n^+(r_l),\ n \in [0, N/2],\ l \in [1, M]$ as defined by equation (4.14):
   (a) Set $u_n^+(r_M) = 0,\ n \in [0, N/2]$,
   (b) For $l = M-1, \cdots, 1$, compute
   $$u_n^+(r_l) = \left(\frac{r_l}{r_{l+1}}\right)^n u_n^+(r_{l+1}) + D_n^{l,l+1}, \quad n \in [0, N/2].$$

5. Compute the Fourier coefficients $u_n(r_l),\ n \in [-N/2, N/2],\ l \in [1, M]$ by combining coefficients $u_n^-(r_l)$ and $u_n^+(r_l)$ as in equation (4.15).
   For $l = 1, 2, \cdots, M$, compute
   $$u_n(r_l) = u_n^-(r_l) + \overline{u_{-n}^+(r_l)}, \quad n \in [-N/2, -1],$$
   $$u_0(r_l) = \overline{\log(r_l)} u_0^-(r_l) + u_0^+(r_l),$$
   $$u_n(r_l) = \overline{u_{-n}(r_l)}, \quad n \in [1, N/2].$$

6. Compute the solution values $u(r_l e^{i\theta_k}), l \in [1, M], k \in [1, N]$ from the Fourier coefficients $u_n(r_l), l \in [1, M], n \in [-N/2, N/2]$. FFT is used for such purposes as discussed at the end of next subsection.

4.2 Solution of the Problem (4.5)

The solution for the harmonic function $v(r, \theta)$ in the annular domain D satisfying the Dirichlet boundary conditions (see equations (4.5)) can be represented as an infinite series. This solution is available in many elementary books in partial differential equations and/or applied mathematics. Below, we present this solution as a theorem for the sake of completeness.

Theorem 2. *Let a_n and b_n be the nth Fourier coefficients of boundary functions $h_1(\theta)$ and $h_2(\theta)$ defined by*

$$h_1(\theta) = g_1(\theta) - u(\beta_1, \theta) \quad \textit{and} \quad h_2(\theta) = g_2(\theta) - u(\beta_2, \theta). \tag{4.16}$$

Then the Fourier coefficients $v_n(r)$ of the solution $v(r, \theta)$ of (4.5) are given by

$$v_n(r) = \begin{cases} C_0 \ln r + D_0, & \textit{if } n = 0, \\ C_n r^{-n} + D_n r^n, & \textit{if } n \neq 0, \end{cases} \tag{4.17}$$

where

$$C_0 = \frac{a_0 - b_0}{\ln(\beta_1/\beta_2)} \quad \textit{and} \quad D_0 = \frac{b_0 \ln \beta_1 - a_0 \ln \beta_2}{\ln(\beta_1/\beta_2)}, \tag{4.18}$$

and

$$C_n = \frac{\beta_1^n \beta_2^n (b_n \beta_1^n - a_n \beta_2^n)}{(\beta_1^{2n} - \beta_2^{2n})} \quad \textit{and} \quad D_n = \frac{(a_n \beta_1^n - b_n \beta_2^n)}{(\beta_1^{2n} - \beta_2^{2n})}. \tag{4.19}$$

Algorithm 2: Computation of Solution of Equation (4.5) in the Annular Domain *D*.

For a given grid size $M \times N$, equidistant grid points $(r_l = \beta_2 + (l-1)(\beta_1 - \beta_2)/(M-1), \theta_k = 2\pi k/N)$, and boundary values $h_1(\theta_k)$ and $h_2(\theta_k)$, the algorithm returns the solution values $v(r_l e^{\theta_k}), l \in [1, M], k \in [1, N]$.

1. Compute the Fourier coefficients a_n and $b_n,\ n \in [-N/2, N/2]$, of the boundary data $h_1(\theta_k)$ and $h_2(\theta_k),\ k \in [1, N]$. FFT is used for such purposes as discussed in the note below.

2. Compute the coefficients C_n and D_n, $n \in [-N/2, N/2]$ using equations (4.18) and (4.19).

3. Compute the Fourier coefficients $v_n(r_l)$, $n \in [-N/2, N/2]$, $l \in [1, M]$ for the solution $v(r, \theta)$ using equation (4.17).

4. Compute the solution values $v(r_l e^{i\theta_k}), l \in [1, M], k \in [1, N]$ from the Fourier coefficients $v_n(r_l), l \in [1, M], n \in [-N/2, N/2]$. FFT is used for such purposes as discussed in the note below.

Finally, we add the solutions obtained from Algorithm-1 for equation (4.4) and from Algorithm-2 for problem (4.4) to obtain the desired solution of the problem (4.1).

Note: In Algorithms 1 and 2, we use FFT's of length N, which is a power of 2, in going back and forth between the data and its Fourier coefficients. This requires obvious slight modification of these algorithms such as using $n \in [-N/2 - 1, N/2]$ instead of using $n \in [-N/2, N/2]$. This requires careful implementation of the method.

4.3 The Computational Complexity of the Algorithm

In steps 1 and 5 of Algorithm-1, there are 2M FFT's of length N and all other computations in steps 2, 3, and 4 are of lower order. Similarly, in steps 1 and 4 of Algorithm-2, there are 2M FFT's of length N and all other computations in steps 2 and 3 are of lower order. With each FFT of length N contributing $N \ln N$ operations, the asymptotic operation count and hence the asymptotic time complexity is $O(MN \ln N)$. It is easy to see that the asymptotic storage requirement is of the order $O(MN)$. Finally, we remark that the above algorithms are parallelizable on multi processor machines (see Borges and Daripa [3] for details).

5 Numerical Results and Discussions

The numerical method presented in the previous section has been implemented for modeling the pulsatile blood flow in an eccentric catheterized artery which involves the following assumptions: (i) the arterial segment is straight, (ii) the arterial wall is rigid and impermeable, (iii) blood is an incompressible Newtonian fluid, and (iv) the flow is fully developed. The flux (flow rate) $Q(t)$ is considered to be a prescribed periodic function of time t. With these assumptions and conditions, the numerical results for the axial pressure gradient $\frac{\partial p}{\partial z}(t)$ and the axial velocity distribution $w(x, y, t)$ are obtained for different values of the Womersley frequency parameter α, radii ratio a, and eccentricity parameter c. These results are used to obtain the estimates of the increased mean pressure gradient and frictional resistance in the artery due to the insertion of a catheter into it.

The model problem in Fourier space reduces to solving two coupled Poisson equations (3.16) with Dirichlet boundary conditions (3.17), for each Fourier mode $j \in [-K, K]$, where K is the number of harmonics in the Fourier series representation of the prescribed periodic flow rate $Q(t)$ (see below for the representation of flow rate); K is assigned the value 6. These Dirichlet problems are solved iteratively using the scheme (3.18) and (3.19) and convergence criterion (3.20). The value of ϵ in equation (3.20) is chosen as 10^{-6}. For better accuracy of the numerical results, the number of grid points $M + 1$ in the radial directions is chosen as 101 and the number of grid points N in the angular direction is chosen as 128. It is found that the convergence of the iterative scheme for higher values of the Fourier modes j depends very much on the values of the Womersley frequency parameter α, radii ratio a, and eccentricity parameter c. The values of a and c are chosen to satisfy $a < 1$, $c > 0$ and $a + c < 1$. For larger values of a and smaller values of c, the iterative scheme converges for a large range of values of α. But, for smaller values of a and larger values of c, the scheme is very sensitive to values of α and converges for relatively smaller values of α. For $\alpha \leq 1$, the scheme converges for all $j \in [-6, 6]$ and for almost all values of a and c in the above range.

Figure 2 shows the curve for time variation of flow rate $Q(t)$ in a cycle of oscillation that is used to compute the axial pressure gradient $\frac{\partial p}{\partial z}(t)$ and the axial velocity distribution $w(x, y, t)$ in the eccentric catheterized artery for different values of the parameters α, a, and c. This curve represents an approximation to a measured flow rate in a canine femoral artery (see MacDonald [11]). It is specified by the equation

$$Q(t) = \sum_{j=0}^{6} Q_j^* \cos(jt - \psi_j), \tag{5.1}$$

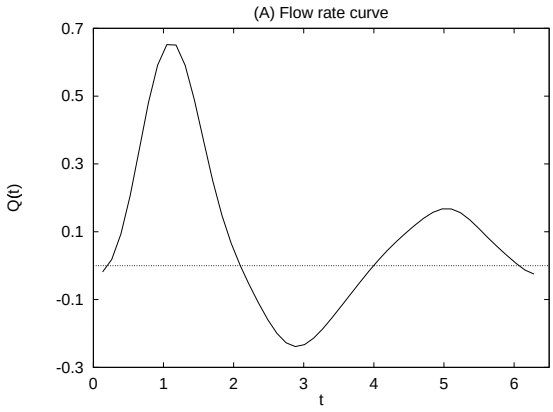

Figure 2: Time variation of flow rate $Q(t)$ during a cycle of oscillation.

where Q_j^* and ψ_j, $j = 0, 1, \cdots, 6$, are the amplitudes and moduli of the harmonics of the flow rate $Q(t)$ which are specified in Table 1. The series (5.1) can be written in the form of complex Fourier series (2.7) if we define

$$Q_0 = Q_0^* \cos(\psi_0), \quad Q_j = \frac{1}{2} Q_j^* e^{-i\psi_j}, \quad \text{and} \quad Q_{-j} = \overline{Q_j}, \quad j > 0. \tag{5.2}$$

Table 1: The amplitudes and moduli of the harmonics of the flow rate $Q(t)$ which is defined by equation (5.1) and shown in Figure 2.

j	0	1	2	3	4	5	6
Q_j^*	0.0916	0.2040	0.2292	0.1011	0.0464	0.0291	0.0106
ψ_j	0.0	0.5482	2.6100	3.4670	4.1670	5.3035	6.2832

The behavior of the computed solution E_j of the Dirichlet problem (3.10) and (3.11) is described through Figure 3. This figure actually shows the plots of $|F_j|$ vs. j for different values of α in Figure 3(A) and Figure 3(B): (A) $a = 0.5$, $c = 0.25$ and (B) $a = 0.75$, $c = 0.15$; and for different values of c in Figure 3(C) and Figure 3(D): (C) $\alpha = 1$, $a = 0.25$ and (D) $\alpha = 1$, $a = 0.5$. Here the variables F_j's are related to the functions $E_j(r, \theta)$'s by

$$F_j = \int_0^{2\pi} \int_{\beta_2}^{\beta_1} F(r, \theta) E_j(r, \theta) r dr d\theta. \tag{5.3}$$

Therefore F_j represents the denominator in equation (3.14). The value of F_j depends on four parameters: the specific mode j, Womersley frequency parameter α, the radii ratio a (i.e. the radius of the catheter tube), and the eccentricity parameter c (i.e. the distance of the axis of the catheter tube from the axis of the artery). These dependencies can be inferred directly from the various plots in Figure 3. For example, we notice the following from this figure: (a) $\frac{\partial |F_j|}{\partial \alpha} < 0$, i.e., the magnitude of F_j decreases with an increasing value of α for a fixed value of j, a, and c; but (b) $\frac{\partial |F_j|}{\partial c} > 0$, i.e., the $|F_j|$ increases with increasing value of c; (c) $\frac{\partial |F_j|}{\partial a} < 0$, i.e., the $|F_j|$ decreases with increasing value of a; and finally (d) $\frac{\partial |F_j|}{\partial j} < 0$, i.e., the $|F_j|$ decreases with increasing value of j. We also notice that for smaller values of c and α, the variation of $|F_j|$ with j is negligibly small. The case (c) above is consistent with the fact that cross-sectional area of the catheterized artery decreases with the increase in radii ratio a.

The variation of pressure gradient $\frac{\partial p}{\partial z}(t)$ with time t during a cycle of oscillation for different values of α with (A) $a = 0.5$, $c = 0.25$, and (B) $a = 0.75$, $c = 0.15$; and for different values of c with (C) $\alpha = 1.0$, $a = 0.25$, and (D) $\alpha = 1.0$, $a = 0.5$ is shown in Figure 4. This pressure gradient is computed through equations (3.1) and (3.14). This is the amount of pressure gradient required in the catheterized artery so that the resulting flux in the catheterized artery will be equal to the flux $Q(t)$ in the uncatheterized artery as given by equation (5.1). Therefore, from Figure 4 we can estimate the increase in the pressure gradient in the artery due to catheterization.

It is observed from Figure 4 that the pressure gradient $\frac{\partial p}{\partial z}(t)$ shows the qualitative behavior of the prescribed flow rate $Q(t)$. However, unlike flow rate, it quantitatively varies significantly during a cycle of oscillation. These

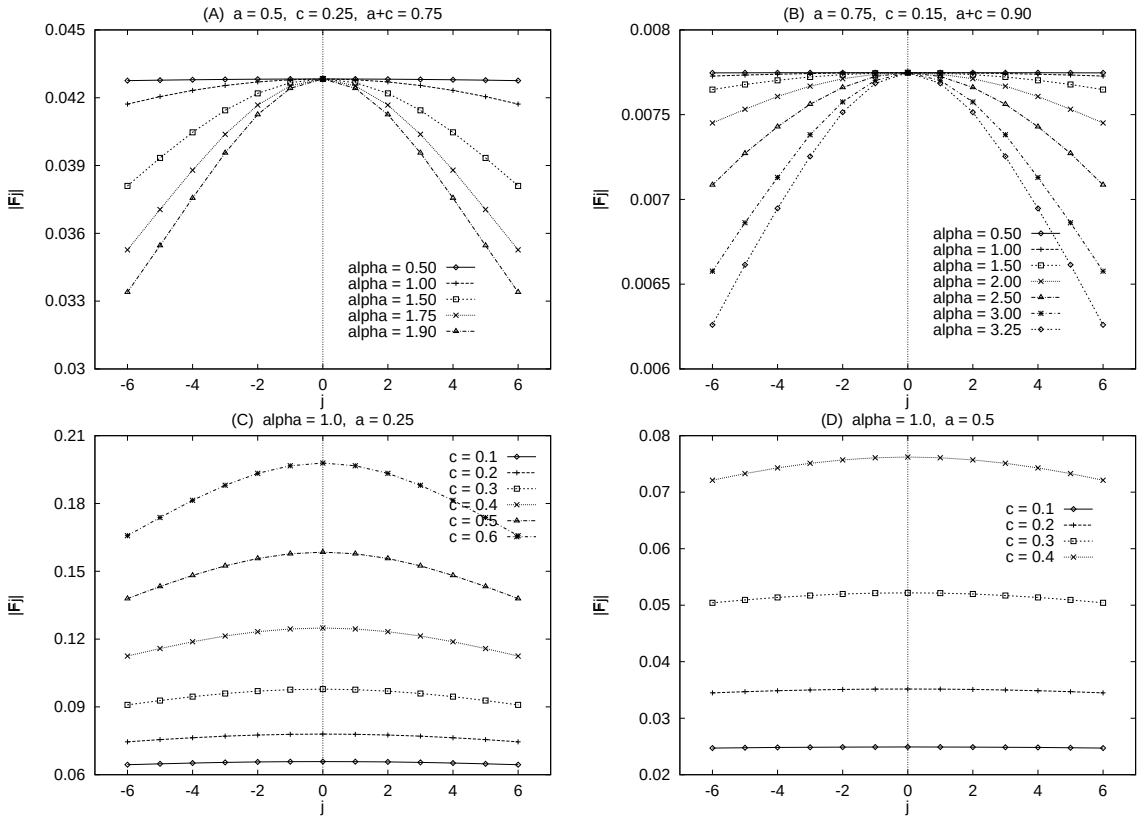

Figure 3: Plots of $|F_j|$ vs. j: plots in (A) and (B) are for different values of α with (A) $a = 0.5$, $c = 0.25$ and (B) $a = 0.75$, $c = 0.15$; plots in (C) and (D) are for different values of c with (C) $\alpha = 1$, $a = 0.25$ and (D) $\alpha = 1$, $a = 0.5$.

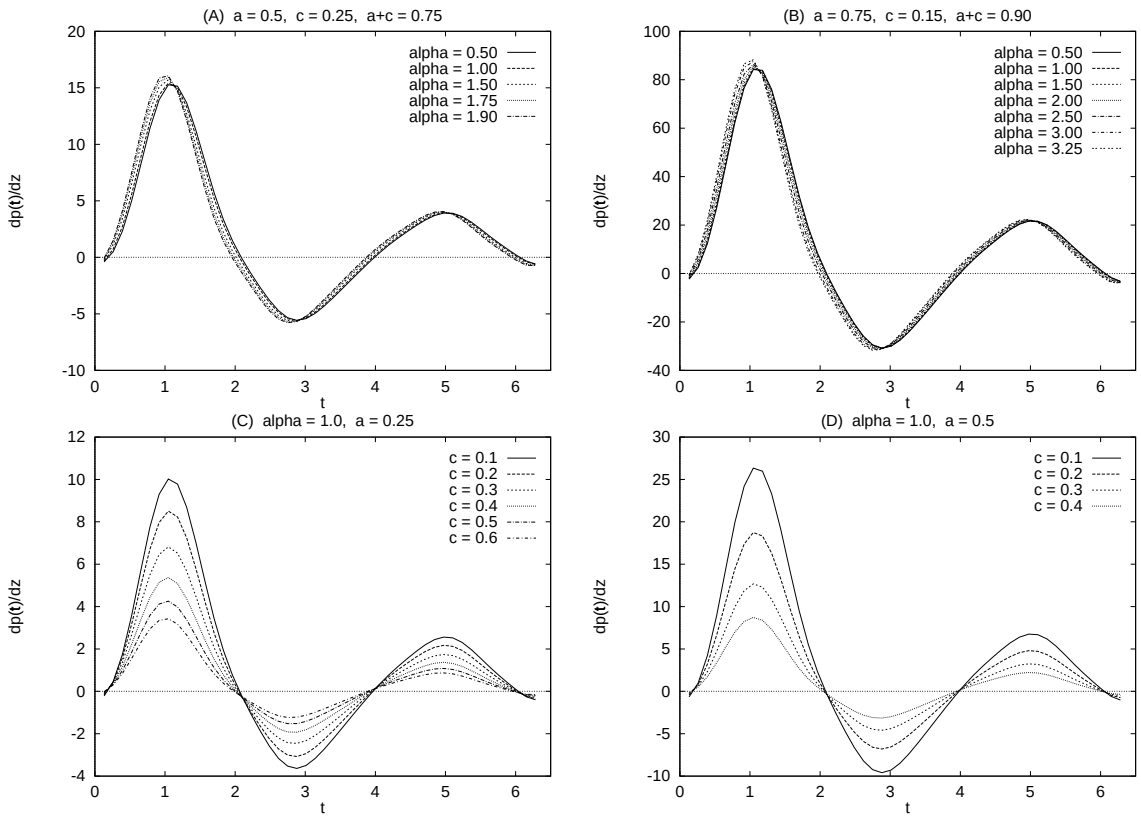

Figure 4: Time variation of pressure gradient $\frac{\partial p}{\partial z}(t)$ during a cycle of oscillation: plots in (A),(B) for different values of α with (A) $a = 0.5$, $c = 0.25$ and (B) $a = 0.75$ and $c = 0.15$, and plots in (C),(D) for different values of c with (C) $\alpha = 1.0$, $a = 0.25$ and (D) $\alpha = 1.0$, $a = 0.5$.

results are in excellent agreement with the results of MacDonald [11]. From Figures 4(A) and 4(B), it is seen that the pressure gradient does not vary appreciably with the Womersley frequency parameter α. However, it varies markedly with the radii ratio a and eccentricity parameter c during a cycle of oscillation: (i) for $a = 0.5$ and $c = 0.25$, the peak pressure gradient is about 15; (ii) where as for $a = 0.75$ and $c = 0.15$, it is about 85 (see Figures 4(A) and 4(B)). Figures 4(C) and 4(D) show that the pressure gradient increases with increasing radii ratio a (or equivalently, the catheter radius), but decreases with increasing eccentricity parameter c (or equivalently, the separation between the center of catheter and the center of artery).

Table 2: The mean (time average over a cycle of oscillation) axial pressure gradient ($\frac{\partial \tilde{p}}{\partial z}$) in the catheterized artery as a function of radii ratio a and eccentricity parameter c with Womersley frequency parameter $\alpha = 1.0$ (The mean flow rate is $Q_0 = Q_0^* \cos(\psi_0) = Q_0^* = 0.0916$).

$c \backslash a$	0.1	0.2	0.3	0.4	0.5	0.6	0.7
0.1	0.899	1.194	1.640	2.371	3.677	6.255	12.051
0.2	0.804	1.030	1.350	1.835	2.605	3.893	6.177
0.3	0.687	0.841	1.047	1.337	1.755	2.376	–
0.4	0.574	0.674	0.802	0.972	1.201	–	–
0.5	0.477	0.541	0.620	0.721	–	–	–
0.6	0.400	0.440	0.488	–	–	–	–

The time averaged mean axial pressure gradient $\frac{\partial \tilde{p}}{\partial z}$ in the catheterized artery obtained as a function of radii ratio a and eccentricity parameter c is presented in Tables 2. The Womersley frequency parameter α is fixed at 1.0. The void entries in this table indicate that the computation has not been done for values of a and c for which $a + c > 0.9$. The time averaged mean flow rate $\tilde{Q}$ obtained from equation (5.1) is 0.0916. The mean frictional resistance is calculated from these tables as the ratio of the mean pressure gradient and the mean flow

rate. So, this table basically indicates how the mean axial pressure gradient and the mean frictional resistance will vary with the radii ratio a and eccentricity parameter c when a catheter is inserted into the artery. The factor by which the mean pressure gradient, or equivalently, the mean frictional resistance increases due to catheterization can be calculated from this table.

6 Concluding Remarks

The fast algorithm of Borges and Daripa [3] for Dirichlet problems in a circular disk is extended here for solving Dirichlet problems in an annular disk. This fast algorithm is implemented and applied to study pulsatile (oscillatory) blood flow in a straight eccentric catheterized artery by modeling blood as an incompressible Newtonian fluid. The axial pressure gradient $\frac{\partial p}{\partial z}(t)$ and the axial velocity distributions $w(x, y, t)$ in the catheterized artery are obtained as solutions of the problem by prescribing the flow rate $Q(t)$ as a suitable periodic function of time t typical of that of a canine femoral artery. Numerical results are obtained for various values of the Womersley frequency parameter α, radii ratio a, and eccentricity parameter c. From these numerical results, changes in the mean pressure gradient and the mean frictional resistance due to the insertion of a catheter into an artery are estimated. These estimates can be used to correct the error involved in the measured pressure gradients using catheters.

The present study shows that axial pressure gradient in the catheterized artery does not vary appreciably with the Womersley frequency parameter α. However, it varies significantly with the radii ratio a (i.e., the catheter radius) and the eccentricity parameter c (i.e., the distance between the center of catheter and the center of artery). The mean axial pressure gradient and the mean frictional resistance increase with increasing catheter radius, but decrease with increasing distance between the center of catheter and the center of artery.

Acknowledgment: This Material is based in part upon work supported by the Texas Advanced Research Program under Grant No. TARP-97010366-030.

References

[1] Back, L.H., "Estimated mean flow resistance increase during coronary artery catheterization", Jour. Biomech. **27** (1994), 169-175.

[2] Back, L.H., Kwack, E.Y., and Back, M.R., "Flow rate-pressure drop relation in coronary angioplasty: catheter obstruction effect", Jour. Biomech. Engng., Trans. ASME **118** (1996), 83-89.

[3] Borges, L., and Daripa, P., "A fast parallel algorithm for the Poisson equation on a disk", Jour. Comput. Phys. (submitted).

[4] Daripa, P., "A fast algorithm to solve nonhomogeneous Cauchy-Riemann equations in the complex plane", SIAM Jour. Sci. Stat. Comput. **13** (1992), 1418-1432.

[5] Daripa, P., and Mashat, D., "Singular integral transforms and fast algorithms", Numer. Algor. **18** (1998), 133-157.

[6] Daripa, P., and Dash, R.K., "An application of a fast algorithm to study oscillatory blood flow in an eccentric catheterized artery," Submitted.

[7] Dash, R.K., Jayaraman, G., and Mehta, K.N., "Estimation of increased flow resistance in a narrow catheterized artery - a theoretical model", Jour. Biomech. **29** (1996), 917-930.

[8] Dash, R.K., Jayaraman, G., and Mehta, K.N., "Flow in a catheterized curved artery with Stenosis", Jour. Biomech. **32** (1999), 917-930.

[9] Jayaraman, G., and Tiwari, K., "Flow in a catheterized curved artery", Med. & Biol. Engng. & Compt. **33** (1995), 1-6.

[10] Karahalios, G.T., "Some possible effects of a catheter on the arterial wall", Med. Phys. **17** (1990), 922-925.

[11] MacDonald, D.A., "Pulsatile flow in a catheterized artery", Jour. Biomech. **19** (1986), 239-249.